# In-plane free vibration of circular and annular FG disks

**†*Y. Yang[1], K.P. Kou[1], C.C. Lam[1]**

[1]Department of Civil and Environmental Engineering, University of Macau, Macau, China.

*Presenting and †Corresponding author: yangyang.liju@hotmail.com

## Abstract

Analysis of the in-plane free vibration of the circular and annular functionally graded disks by a meshfree boundary-domain integral equation method are presented in this paper. The material properties of the disks are assumed to vary in the radial direction obeying an exponential law. Based on the two-dimensional linear elastic theory, the motion equations of the FG disks are derived by using the static fundamental solutions. Radial integration method as an efficient tool is adopted to treat the domain integrals which raised due to the material inhomogeneous and inertial effects. The natural frequencies and associate mode shapes are calculated for the FG disks with combinations of free and clamped boundary conditions. Parametric studies are also conducted to study the effects of the material gradients, radius ratios and boundary conditions on the frequency of the FG disks.

**Keywords:** In-plane free vibration, circular and annular FG disks, meshfree boundary-domain integral equation method

## Introduction

Circular and annular structures are structural components and commonly used in a wide variety of engineering applications including space structures, electronic components and rotating machinery. A lot of attentions have been focus on the free vibration characteristics of circular structures. For example, Weisensel [1] given the results of an extensive literature search and review of available source of numerical natural frequency information for stationary circular and annular elastic plates, where the information regarding the specific plate theory, boundary conditions, geometric properties and material properties used to determine the natural frequency information. Kirkhope and Wilson [2] applied the finite element method to the stress and vibration analysis of thin rotating discs. Han and Liew [3] presented a numerical analysis of the axisymmetric free vibration of moderately thick annular plates using the differential quadrature method (DQM). Chung et al. [4] derived the governing equation for free vibration of a spinning circular disk by using the variational formulation based upon the Kirchhoff plate theory and von Karman strain one, this was because they found that during the derivation that the governing equation was theoretically valid under the assumption that in-plane deflections were steady and axisymmetric, and that internal forces were linearized while the strains remain nonlinear.

In-plane vibration characteristics are also very important for the circular annular structures. As the circular structures in most applications have direct in-plane forces or in-plane force components due to imperfections in the manufacturing, assembly or alignment of the supporting mounts. However, the studies reported on the in-plane vibrations of circular annular disks is relatively scarce. Ambati [5] carried out the in-plane vibrations of annular rings. Nigh and Olson [6] used a finite element formulation for the analysis of rotating disks in either a body-fixed or a space-fixed co-ordinate system. The in-plane stress distribution resulting from the in-plane body force due to rotation was determined first by a plane stress finite element analysis. Farag and Pan [7] analyzed the modal characteristics of in-plane vibrations of a solid disk with clamped outer edge. Park [8] derived the frequency equation for the in-plane vibration of the clamped circular plate of uniform thickness by using Hamilton's principle. The in-plane free vibration of an elastic and isotropic disk was studied by Bashmal et al. [9] on the basis of the two-dimensional linear plane stress theory of elasticity. rie et al. [10] examined the in-plane vibrations in circular and annular disks using transfer matrix formulation. Natural frequencies were obtained for several radius ratios of annular disks with combinations of free and clamped conditions at the inner and outer edges but mode shapes were not presented.

With the increased application of the FG structures, vibration analyses of the FG circular and annular structures have attracted intensive research. Based on the first-order shear deformation theory, Francesco Tornabene [11] presented the dynamic behavior of moderately thick FG conical, cylindrical shells and annular plates, which material properties were graded through the thickness direction. Kermani et al. [12] analyzed the three-dimensional free vibrations of multi-directional graded circular and annular plates by the state space based differential quadrature method, which solved dimensionless equations of motion analytically along thickness direction and numerically along radial direction of the plate. Based on the three-dimensional theory of elasticity, the free and forced vibration analysis of FG circular plate with various boundary conditions was carried out by Nie and Zhong [13], the material properties were assumed to be graded in the thickness direction according to an exponential distribution. Three-dimensional free vibration analysis of FG annular plate were done by Dong [14] using the Chebyshev-Ritz method. The material properties also only varied in the thickness direction. The free vibration analysis of FG thick annular plates subjected to thermal environment was studied by Malekzadeh [15] based on the 3D elasticity theory, the material properties were assumed to be temperature dependent and graded in the thickness direction. Most of the mentioned reference were based on the three-dimensional analysis, and the material properties were only graded in the thickness direction. The other in-plane vibration of the FG circular and annular disks are very rare in the literature. Therefore, an accurate analysis of the in-plane vibration of the FG circular and annular disks with varied material properties in space coordinates must be considered.

Thus, in-plane free vibration of the circular and annular functionally graded disks were presented in this paper. The material properties of the disks were assumed to grade in the radial direction. Based on the two-dimensional linear elastic theory, the motion equations of the FG disks could be derived by a meshfree boundary-domain integral equation method, and the radial integration method was applied to transform the domain integrals into boundary integrals. Normalized natural frequencies were obtained to compare with data available in the literature. Mode shapes were presented to illustrate the free vibration behavior of the disks.

## Geometrical and material properties of circular and annular FG disks

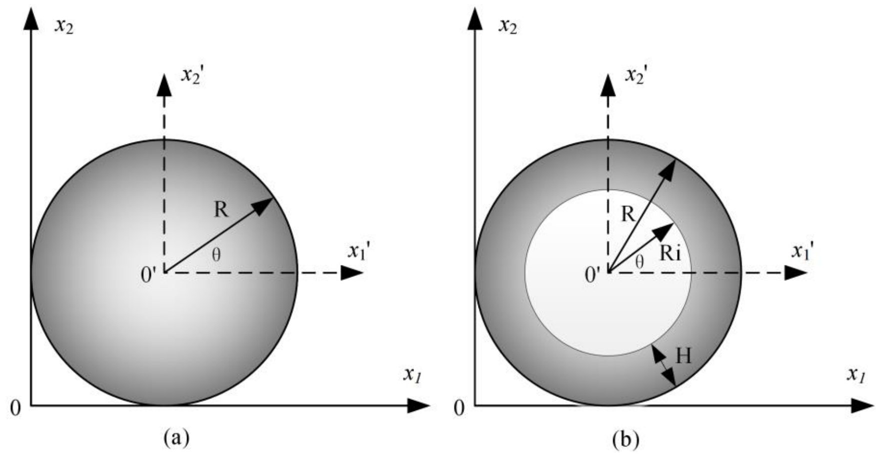


**Figure 1 The geometry coordinates of the circular and annular FG disks**

The considered circular and annular FG disks are displayed in Fig. 1. $R$ is the radius of the circular disk. For the annular FG disk, the outer and the inner radius are $R$ and $R_i$ respectively, and thickness is H. For commen multi-FG disks, the material properties are a function of polar coordinates ($\check{r}$, $\theta$) and vary continuously in one or more directions. In the present paper, only the material properties of the disks grade in radial directions was considered. The Young's modulus $E$ and the density $\rho$ were assumed to vary continuous along the radial direction obeying an exponential law as shown in Eqs. (1) and (2) and the Poisson's ratio $v$ was taking as a constant [16].

$$E = E_s e^{\beta \check{r}}, \qquad \text{where} \qquad \beta = \frac{1}{R - R_i} ln(\frac{E_e}{E_s}), \tag{1}$$

$$\rho = \rho_s e^{\gamma \check{r}}, \qquad \text{where} \qquad \gamma = \frac{1}{R - R_i} ln(\frac{\rho_e}{\rho_s}), \tag{2}$$

$$\text{where} \qquad \check{r} = \sqrt{(x - x_0)^2 + (y - y_0)^2}, \tag{3}$$

where $E_s$ and $\rho_s$ are the Young's modulus and density at the starting face, $E_e$ and $\rho_e$ are the Young's modulus and mass density at the ending face, $\beta$ and $\gamma$ represent the material gradient parameters for Young's modulus and mass density respectively, $\check{r}$ stands for the radial coordinate, $x_0$ and $y_0$ are the center Cartesian coordinates of the considered circular and annular disks.

## Problem formulation

Based on 2D elasticity theory, considering a FG circular disk, the governing differential equation of the steady-state elastodynamics is expressed as

$$\sigma_{ij,j}(\boldsymbol{x}) + \omega^2 \rho u_i(\boldsymbol{x}) = 0. \tag{4}$$

The stress tensor $\sigma_{ij}$ and the displacement vector $u_i$ in Eq. (4) are functions of spatial coordinates $\boldsymbol{x}$. By taking the elastostatic displacement fundamental solutions $U_{ij}(\boldsymbol{x}, \boldsymbol{y})$ as the weight function, the weak-form of the equilibrium Eq. (4) can be obtained by

$$\int_\Omega [\sigma_{jk,k} + \omega^2 \rho u_j] \cdot U_{ij} d\Omega = 0. \tag{5}$$

Substituting the generalized Hooke's law $\sigma_{ij} = c_{ijkl}u_{k,l} = \mu(\boldsymbol{x})c^0_{ijkl}u_{k,l}$ and applying the Gauss's divergence theorem, the weak form yields the following boundary-domain integral equations

$$\begin{aligned}\tilde{u}_i(\boldsymbol{y}) &= \int_\Gamma U_{ij}(\boldsymbol{x},\boldsymbol{y})t_j(\boldsymbol{x})d\Gamma - \int_\Gamma T_{ij}(\boldsymbol{x},\boldsymbol{y})\tilde{u}_j(\boldsymbol{x})d\Gamma + \int_\Omega V_{ij}(\boldsymbol{x},\boldsymbol{y})\tilde{u}_j(\boldsymbol{x})d\Omega \\ &+\omega^2\int_\Omega \frac{\rho(\boldsymbol{x})}{\mu(\boldsymbol{x})}U_{ij}(\boldsymbol{x},\boldsymbol{y})\tilde{u}_j(\boldsymbol{x})d\Omega\end{aligned} \quad . \tag{6}$$

In Eq. (6), the traction vector $t_i = \sigma_{ij}n_j$ and $n_j$ is the components of the outward unit vector normal to the boundary Γ of the considered layer domain Ω. $\tilde{u}_i$ is the normalized displacement vector associated with the normalized shear modulus $\tilde{\mu}$, as defined by [17]

$$\tilde{u}_i(\boldsymbol{x}) = \mu(\boldsymbol{x})u_i(\boldsymbol{x}), \qquad \tilde{\mu}(\boldsymbol{x}) = \ln[\mu(\boldsymbol{x})]. \tag{7a, b}$$

where the shear modulus $\mu(\boldsymbol{x})$ varies with the coordinates, and is related to the Young's modulus by $\mu(\boldsymbol{x}) = E(\boldsymbol{x})/2(1+v)$.
The ratio of the density and shear modulus in Eq. (6) is expressed as $\frac{\rho(\boldsymbol{x})}{\mu(\boldsymbol{x})} = \frac{\rho_s}{\mu_s}e^{(\gamma-\beta)\sqrt{(x-x_0)^2+(y-y_0)^2}}$.

$U_{ij}(\boldsymbol{x},\boldsymbol{y})$ and $T_{ij}(\boldsymbol{x},\boldsymbol{y})$ are the elastostatic displacement fundamental solutions for homogeneous, isotropic and linear elastic solids with $\mu$=1 [18].

$$U_{ij} = \frac{-1}{8\pi(1-v)}[(3-4v)\delta_{ij}\ln(r) - r_{,i}r_{,j}], \tag{8}$$

$$\Sigma_{ijl} = c^0_{rsjl}U_{ir,s} = \frac{-1}{4\pi(1-v)r}[(1-2v)(\delta_{il}r_{,j} + \delta_{ij}r_{,l} - \delta_{jl}r_{,i}) + 2r_{,i}r_{,j}r_{,l}], \tag{9}$$

$$T_{ij} = \Sigma_{ijl}n_l = \frac{-1}{4\pi(1-v)r}[(1-2v)(n_ir_{,j} - n_jr_{,i}) + ((1-2v)\delta_{ij} + 2r_{,i}r_{,j})r_{,l}n_l], \tag{10}$$

$$V_{ij} = \Sigma_{ijl}\tilde{\mu}_{,l} = \frac{-1}{4\pi(1-v)r}[(1-2v)(\tilde{\mu}_{,i}r_{,j} - \tilde{\mu}_{,j}r_{,i}) + ((1-2v)\delta_{ij} + 2r_{,i}r_{,j})r_{,l}\tilde{\mu}_{,l}], \tag{11}$$

where $\delta_{ij}$ is the Kronecker delta. $r=|\boldsymbol{x}-\boldsymbol{y}|$ is the distance from the field point $\boldsymbol{x}$ to the source point $\boldsymbol{y}$. The elasticity tensor $c_{ijkl}$ can be described in the form of

$$c_{ijkl}(\boldsymbol{x}) = \mu(\boldsymbol{x})c^0_{ijkl}, \quad \text{where} \quad c^0_{ijkl} = \frac{2v}{1-2v}\delta_{ij}\delta_{kl} + \delta_{ik}\delta_{jl} + \delta_{il}\delta_{jk}, \tag{12a, b}$$

where $c^0_{ijkl}$ is the elasticity tensor for the corresponding "fictitious" homogeneous material with $\mu$=1.

One to be noted is that, the $\tilde{\mu}_{,l}$ in Eq.(11) is not constant any more, it yields:

$$\tilde{\mu}_{,l} = \beta\left[(x-x_0)^2 + (y-y_0)^2\right]^{-\frac{1}{2}}(x-x_0), \qquad \text{where } l=1, \tag{13a}$$

$$\tilde{\mu}_{,l} = \beta\left[(x-x_0)^2 + (y-y_0)^2\right]^{-\frac{1}{2}}(y-y_0), \qquad \text{where } l=2. \tag{13b}$$

Boundary-domain integral equations for boundary points can be obtained by locating $\boldsymbol{y}$ at the boundary $\Gamma$ in Eq. (6). It is observed that the two domain integrals in the Eq. (6) arise from the material inhomogeneity and the inertial effect. Radial integration method (RIM) of Gao [19] was employed to transform the domain integrals into boundary integrals over the global boundary. The normalized displacements is approximated by a combination of the radial basis functions and the polynomials of global coordinates as

$$\tilde{u}_i(\boldsymbol{x}) = \sum_A \alpha_i^A \phi^A(R) + a_i^k x_k + a_i^0, \qquad \sum_A \alpha_i^A = 0, \qquad \sum_A \alpha_i^A x_j^A = 0, \tag{14a, b, c}$$

where $\phi^A(R)$ is the radial basis function, $\alpha_i^A$, $a_i^k$ and $a_i^0$ are unknown coefficients to be determined, $x_k$ and $x_j^A$ denote the coordinates of the field point $\boldsymbol{x}$ and the application point $A$ respectively. In this analysis, the following 4th order spline-type radial basis function was applied [20]

$$\phi^A(R) = \begin{cases} 1 - 6\left(\dfrac{R}{d_A}\right)^2 + 8\left(\dfrac{R}{d_A}\right)^3 - 3\left(\dfrac{R}{d_A}\right)^4, 0 \le R \le d_A \\ 0, R \ge d_A \end{cases}, \tag{15}$$

where $R=\|\boldsymbol{x}-\boldsymbol{x}^{\boldsymbol{A}}\|$ is the distance from the application point $A$ to the field point $\boldsymbol{x}$, and $d_A$ is the support size for the application point $A$. The two domain integrals of Eq. (6) are transformed into the boundary integrals in the form of [21]

$$\int_\Omega V_{ij}\tilde{u}_j d\Omega = \alpha_j^A \int_\Gamma \frac{1}{r}\frac{\partial r}{\partial n} F_{ij}^A d\Gamma + a_j^k \int_\Gamma \frac{r_{,k}}{r}\frac{\partial r}{\partial n} F_{ij}^1 d\Gamma + (a_j^k y_k + a_j^0)\int_\Gamma \frac{1}{r}\frac{\partial r}{\partial n} F_{ij}^0 d\Gamma, \tag{16}$$

$$\omega^2 \int_\Omega \frac{\rho}{\mu} U_{ij}\tilde{u}_j d\Omega = \omega^2 \frac{\rho_s}{\mu_s}[\alpha_j^A \int_\Gamma \frac{1}{r}\frac{\partial r}{\partial n} P_{ij}^A d\Gamma + a_j^k \int_\Gamma \frac{r_{,k}}{r}\frac{\partial r}{\partial n} P_{ij}^1 d\Gamma + (a_j^k y_k + a_j^0)\int_\Gamma \frac{1}{r}\frac{\partial r}{\partial n} P_{ij}^0 d\Gamma], \tag{17}$$

where the relation $x_i=y_i+r_{,i}r$ is used to relate $x$ with $r$. By rewriting Eq. (11) with $V_{ij} = \bar{V}_{ij}/r$, the integral functions in Eqs. (16) and (17) can be expressed as

$$F_{ij}^A = \int_0^r rV_{ij}\phi^A dr = \bar{V}_{ij}\int_0^r \phi^A dr, \; F_{ij}^1 = \int_0^r r^2 V_{ij} dr = \frac{1}{2}r^2\bar{V}_{ij}, \; F_{ij}^0 = \int_0^r rV_{ij} dr = r\bar{V}_{ij}, \tag{18a,b,c}$$

$$P_{ij}^A = \int_0^r rU_{ij}\phi^A e^{(\gamma-\beta)\sqrt{(x-x_0)^2+(y-y_0)^2}} dr, \qquad P_{ij}^1 = \int_0^r r^2 U_{ij} e^{(\gamma-\beta)\sqrt{(x-x_0)^2+(y-y_0)^2}} dr,$$

$$P_{ij}^0 = \int_0^r rU_{ij} e^{(\gamma-\beta)\sqrt{(x-x_0)^2+(y-y_0)^2}} dr. \tag{19a,b,c}$$

Since $r_{,i}$ in the above radial integrals is a constant, Eqs. (18b, c) can be evaluated analytically and the other integrals are calculated by standard Gaussian quadrature formula [22, 23]. Therefore the displacement boundary integral equations with only boundary integrals are obtained as

$$\begin{aligned} c_{ij}\tilde{u}_j &= \int_\Gamma U_{ij} t_j d\Gamma - \int_\Gamma T_{ij}\tilde{u}_j d\Gamma + [\alpha_j^A \int_\Gamma \frac{1}{r}\frac{\partial r}{\partial n} F_{ij}^A d\Gamma + a_j^k \int_\Gamma \frac{r_{,k}}{r}\frac{\partial r}{\partial n} F_{ij}^1 d\Gamma \\ &+ (a_j^k y_k + a_j^0)\int_\Gamma \frac{1}{r}\frac{\partial r}{\partial n} F_{ij}^0 d\Gamma] + \omega^2 \frac{\rho_0}{\mu_0}[\alpha_j^A \int_\Gamma \frac{1}{r}\frac{\partial r}{\partial n} P_{ij}^A d\Gamma + a_j^k \int_\Gamma \frac{r_{,k}}{r}\frac{\partial r}{\partial n} P_{ij}^1 d\Gamma \, . \\ &+ (a_j^k y_k + a_j^0)\int_\Gamma \frac{1}{r}\frac{\partial r}{\partial n} P_{ij}^0 d\Gamma] \end{aligned} \tag{20}$$

Discretizing of the boundary with boundary elements and collocating the resulting boundary integral equations at all the boundary and internal nodes yield the following $2N_t$ x $2N_t$ generalized eigenvalue system for free vibration analysis,

$$[\boldsymbol{K}]\{\boldsymbol{X}\} = \omega^2 [\boldsymbol{M}]\{\boldsymbol{X}\}. \tag{21}$$

By solving this general eigenvalue equation, the eigenvalue $\omega$ and the corresponding mode shapes $\{\boldsymbol{X}\}$ can be obtained numerically.

**Numerical verification**

A comparison is made on the in-plane free vibration of an isotropic, homogeneous clamped circular plate with the study by Park [14] using Hamilton's principle. In the comparison, the aluminum plate of a radius of 0.5m and a thickness of 5mm, $E$=71GPa, $\rho$=2700 kg/m$^3$ and $v$=0.33. To validate the analyzed results, the natural frequencies are also computed using the finite element method (FEM). The results of the present method are in good agreement with those of the FEM, which can be seen from the errors listed in Table 1. The present results are also close to the Ref. [8], even though solutions in Ref [8] are not complete, and some values are missing. This may be due to the reason that in Ref. [8], the displacements were assumed as the displacement multiple with a trigonometric function $cosm\theta$ or $sinm\theta$, where $m$=0, 1, 2…, ∞ was the circumferential wave number. The wave number had a correspondence frequency, if interchanging the trigonometric function $cosm\theta$ or $sinm\theta$, another set of free vibration modes can be obtained.

**Table 1 Comparison of natural frequencies of the homogeneous clamped circular disk**

| Mode | Ref. [8] | Present(Hz) | FEM(Hz) | error(%) |
|---|---|---|---|---|
| 1 | 3362 | 3360.1184 | 3360.3 | 0.0054 |
| 2 | - | 3360.1340 | 3360.4 | 0.0079 |
| 3 | 3835 | 3832.3110 | 3830.2 | 0.0551 |
| 4 | 5219 | 5214.3752 | 5211.9 | 0.0475 |
| 5 | - | 5214.3916 | 5212.1 | 0.0439 |
| 6 | 5383 | 5374.0392 | 5369.4 | 0.0863 |
| 7 | - | 5374.0648 | 5369.7 | 0.0812 |
| 8 | 6626 | 6612.1173 | 6617.5 | 0.0814 |
| 9 | 6764 | 6755.7080 | 6743.5 | 0.1807 |
| 10 | - | 6755.7498 | 6743.8 | 0.1769 |
| 11 | 6939 | 6911.3853 | 6911.2 | 0.0027 |
| 12 | - | 6911.3953 | 6913.2 | 0.0261 |
| 13 | 7021 | 6985.4645 | 6990.7 | 0.0749 |
| 14 | - | 8082.0531 | 8084.4 | 0.0290 |
| 15 | - | 8082.2690 | 8089.6 | 0.0907 |
| 16 | 8130 | 8129.7628 | 8091.0 | 0.4768 |
| 17 | - | 8294.3571 | 8273.8 | 0.2478 |
| 18 | - | 8438.0543 | 8435.4 | 0.0315 |
| 19 | - | 8438.1857 | 8437.9 | 0.0034 |
| 20 | 8489 | 8499.8673 | 8512.4 | 0.1474 |
| 21 | - | 8500.4750 | 8514.3 | 0.1626 |

Another comparision is taking on the in-plane free vibration of the isotropic, homogeneous annular disks with several combinations of boundary conditions. The results of the present method are compared with those available in the literature are tabulated in Table 2. Parameter $\eta=Ri/R$ which is the ratio between inner and outer radii of the disk. The boundary conditions were free in inner and clamped in outer circumfrential and are expressed as F-C, and other boundary conditions are deduced from this. To validate the analyzed results, the natural frequencies are also computed using the FEM. It can be obtained that, the normalized natural frequencies calculated by using the present method agreed well with those of FEM and references. However in Refs. [9] and [10], for F-C annular disks, the fundamental natural frequencies is close to the results of present method and FEM, but for the other two boundary conditions annular disks, the fundamental natural frequencies are close to the second frequencies of present method and FEM.

**Table 2 Comparison of non-dimensional fundamental natural frequencies of annular disks**

| Radius ratio(η) | Boundary conditions | Mode | Present | FEM | Ref. [10] | Ref. [9] |
|---|---|---|---|---|---|---|
| 0.2 | F-C | 1 | 2.0802 | 2.0983 | 2.1040 | 2.1060 |
| | C-C | 1 | 2.4801 | 2.4614 | - | - |
| | | 2 | 2.7479 | 2.7347 | 2.7830 | 2.8060 |
| | C-F | 1 | 0.3479 | 0.3444 | - | - |
| | | 2 | 0.9085 | 0.9060 | 0.9190 | 0.9400 |
| 0.4 | F-C | 1 | 2.4365 | 2.4272 | 2.5170 | 2.5220 |
| | C-C | 1 | 3.1449 | 3.1285 | - | - |
| | | 2 | 3.3914 | 3.3607 | 3.4290 | 3.4560 |
| | C-F | 1 | 0.8139 | 0.8105 | - | - |
| | | 2 | 1.2663 | 1.2631 | 1.2810 | 1.2960 |

Since the in-plane free vibration of the circular FG disk are very rare in the literature, the result computed by the present method is compared with that by using FEM and presented in Table 3. In this example, the center of the disk is $x_0$=0.5m, $y_0$=0.5m, and $R$=0.5m, the material perperties are graded from center steel $E$=210GPa, $\rho$=7806kg/m$^3$ along the radial direction to circumference aluminum $E$=70GPa, $\rho$=2707kg/m$^3$. Three kinds of the boundary and internal nodes distribution are taken to investigate the efficiency of the present method and plotted in Fig. 2. From the comparision, it can be seen that, 36 boundary nodes and 73 internal nodes is sufficent to achieve the convergence results even for high frequencies. Increasing the internal nodes can accurate the results, thus the error between the results of the present method with 36 boundary nodes and 145 internal nodes and those of FEM are vary small. The corresponding vibration modes are also obtained by using the presnet method and darwn in Fig. 3.

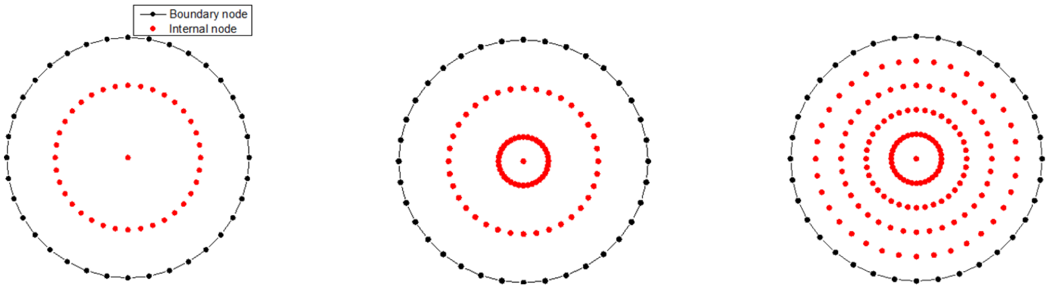


(a) 36B37I (b) 36B73I (c) 36B145I

**Figure 2 Boundary and internal nodes distribution**

**Table 3 Comparison of non-dimensional natural frequencies of circular FG disk**

| Modes | Present | | | FEM | Error(%) |
|---|---|---|---|---|---|
| | 36B37I | 36B73I | 36B145I | | |
| 1 | 1.7544 | 1.7815 | 1.7953 | 1.8196 | 1.3387 |
| 2 | 1.7545 | 1.7816 | 1.7953 | 1.8196 | 1.3385 |
| 3 | 2.1044 | 2.0880 | 2.0832 | 2.0843 | 0.0544 |
| 4 | 3.0696 | 3.1550 | 3.1404 | 3.1494 | 0.2850 |
| 5 | 3.0697 | 3.1551 | 3.1404 | 3.1494 | 0.2846 |
| 6 | 3.2924 | 3.2440 | 3.2331 | 3.2314 | 0.0517 |
| 7 | 3.2924 | 3.2440 | 3.2331 | 3.2314 | 0.0520 |
| 8 | 4.2514 | 4.0276 | 4.0872 | 4.1249 | 0.9123 |
| 9 | 4.2514 | 4.1782 | 4.2033 | 4.2041 | 0.0213 |
| 10 | 4.4116 | 4.1782 | 4.2033 | 4.2041 | 0.0208 |

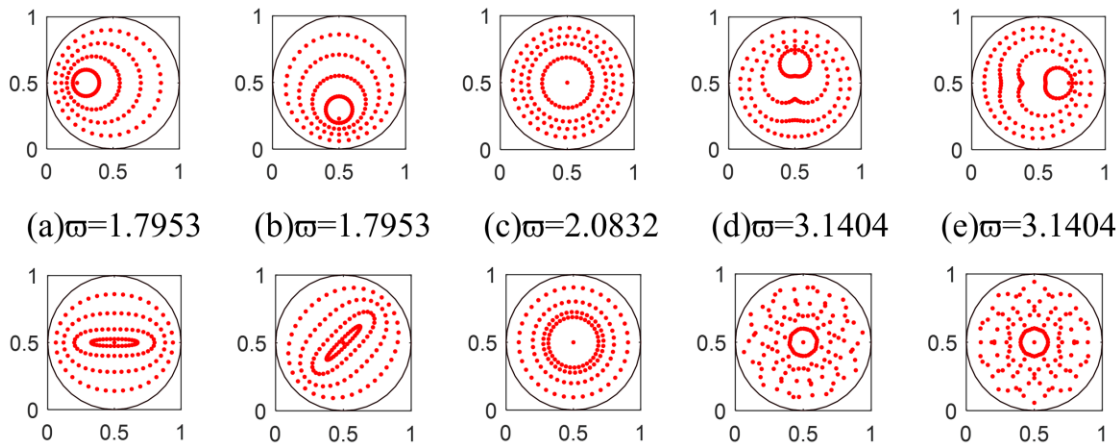

(a)ϖ=1.7953 (b)ϖ=1.7953 (c)ϖ=2.0832 (d)ϖ=3.1404 (e)ϖ=3.1404

(f)ϖ=3.2331 (g)ϖ=3.2331 (h)ϖ=4.0872 (i)ϖ=4.2033 (j)ϖ=4.2033

**Figure 3 First ten mode shapes of clamped circular FG disk**

**Free vibration of the circular and annular FG disks**

In this part, the present method is used to analysis the free vibration of the circular and annular FG disks with kinds of combination of boudary conditions. A steel/aluminum FG material is cosidered for all the numerical analyses, thus the matrterial properties can start from steel or aluminum and grade in the radial direction. For circular disks, the material properties grade from steel in the center to the outer edge aluminum are noted as S-A circular disk, A-S circlar disk means the material properties are grading in an opposite order. S-A annular disk presents the material properties grade from steel in the inner edge to outer aluminum edge. Only clmaped boundary support is taken in FG circular disks analyses. For annular FG disks, the free and clamped conditions at the inner and outer edges are noted as F-C, and so on C-F as well as C-C are also considered in the annular FG disks analysis. All the results were all normalized by $\varpi = \omega\left(R - R_i\right)\sqrt{\frac{\rho_{steel}}{E_{steel}}}$ .

The first five normalized natural frequencies of clamped circular FG disks are shown in Table 4. To compared the circular FG disks with the homogeneous one, the normalized natural frequencies for the steel and aluminum disks are also listed. It can be seen that, the normalized natural frequencies of S-A($\beta$=-1.0986, $\gamma$=-1.0591) < Aluminum($\beta$=0, $\gamma$=0) < Steel($\beta$=0, $\gamma$=0) < A-S($\beta$=1.0986, $\gamma$=1.0591). That is with increasing the material gradients, increase the natural frequencies. For the homogeneous aluminum and steel, the material gradients are all equal to zero, in this case, the harder stiffness leads to the higher natural frequencies. It can be obtained that, by using the corresponding FG materials instead of the homogeneous material, can reduce or increase the natural frequencies of circular disks.

**Table 4 First five normalized natural frequencies of clamped circular FG disks**

| Circular disks | ϖ=1 | ϖ=2 | ϖ=3 | ϖ=4 | ϖ=5 |
|---|---|---|---|---|---|
| S-A | 1.7927 | 1.7927 | 2.0834 | 3.1446 | 3.1446 |
| Aluminum | 2.1590 | 2.1590 | 2.3282 | 3.2802 | 3.2802 |
| Steel | 2.2022 | 2.2022 | 2.3747 | 3.3457 | 3.3457 |
| A-S | 2.5701 | 2.5701 | 2.6300 | 3.5125 | 3.5125 |

**Table 5 First five normalized natural frequencies of kinds of annular FG disks**

| Radius ratio($\eta$) | Modes | F-C | | C-C | | C-F | |
|---|---|---|---|---|---|---|---|
| | | A-S | S-A | A-S | S-A | A-S | S-A |
| 0.2 | 1 | 2.1794 | 1.5050 | 2.3217 | 1.8726 | 0.2073 | 0.4002 |
| | 2 | 2.2668 | 1.5050 | 2.6141 | 2.2271 | 0.6332 | 0.9141 |
| | 3 | 2.2668 | 1.6275 | 2.6141 | 2.2271 | 0.6332 | 0.9141 |
| | 4 | 2.5965 | 1.9757 | 3.1886 | 2.8651 | 1.0528 | 1.5327 |
| | 5 | 2.5965 | 1.9757 | 3.1886 | 2.8652 | 1.0529 | 1.5327 |
| 0.4 | 1 | 1.8157 | 1.2719 | 2.1766 | 1.8283 | 0.3839 | 0.6625 |
| | 2 | 2.0013 | 1.3714 | 2.3598 | 2.0260 | 0.6814 | 0.9398 |
| | 3 | 2.0013 | 1.3714 | 2.3598 | 2.0260 | 0.6814 | 0.9398 |
| | 4 | 2.2527 | 1.5038 | 2.8034 | 2.4727 | 1.0336 | 1.4118 |
| | 5 | 2.2528 | 1.5039 | 2.8034 | 2.4727 | 1.0336 | 1.4118 |

| | | | | | | | |
|---|---|---|---|---|---|---|---|
| | 1 | 1.6742 | 1.0231 | 2.1128 | 1.8465 | 0.5402 | 0.8548 |
| | 2 | 1.8051 | 1.1460 | 2.1790 | 1.8917 | 0.6891 | 0.9553 |
| 0.6 | 3 | 1.8124 | 1.1460 | 2.1790 | 1.8917 | 0.6891 | 0.9553 |
| | 4 | 1.8126 | 1.3464 | 2.3863 | 2.1216 | 0.9729 | 1.2128 |
| | 5 | 1.9151 | 1.3464 | 2.3863 | 2.1216 | 0.9729 | 1.2128 |
| | 1 | 1.2539 | 0.8166 | 2.0318 | 1.7238 | 0.7050 | 0.9582 |
| | 2 | 1.4467 | 0.8234 | 2.0321 | 1.7931 | 0.7479 | 0.9619 |
| 0.8 | 3 | 1.4550 | 0.8234 | 2.1098 | 1.7931 | 0.7479 | 0.9619 |
| | 4 | 1.4551 | 0.9147 | 2.2030 | 1.8054 | 0.8418 | 1.0482 |
| | 5 | 1.5376 | 0.9148 | 2.2030 | 1.8057 | 0.8418 | 1.0482 |

The first five normalized natural frequencies of two kinds of annular FG disks with three boundary conditions as well as four radius ratios are also shown in Table 5. It can be seen that, for F-C and C-C annular FG disks, increasing the annular radius ratio would decrease the natural frequencies, and for the same radius ratio, the higher material gradients give rise to higher natural frequencies. But for C-F annular disks, that is clamped at the inner edge and free at the outer edge, increasing the radius ratio would increase the natural frequencies and the smaller material gradients the higher the natural frequencies, these regularities are all oppositing with that of F-C and C-C annular disks. Thus it can be concluded that, the material gradiens, radius ratios and boundary conditions all affect the free vibration of the annular FG disks a lot.

## Conclusion

In this paper, the free vibration of the circular and annular FG disks were analyzed by a meshfree boundary-domain integral equation methods. The material properties were graded along the radial direction from center or inner edge to outer edge for circular and annular disks respectively. From the numerical analyses, it can be concluded that, the present method has fast convergence, high efficiency and accuracy.

## Acknowledge

This project is supported by the RDAO of University of Macau (RADO Project no: MYRG2015-00142-FST).

### References


[1] Weisensel GN. Natural frequency information for circular and annular plates. Journal of Sound and Vibration, 1989, 133(1): 129-137.

[2] Kirkhope J, Wilson GJ. Vibration and stress analysis of thin rotating discs using annular finite elements. Journal of Sound and Vibration, 1976, 44(4): 461-474.

[3] Han JB, Liew KM. Axisymmetric free vibration of thick annular plates, International Jounral of Mechanical Sciences, 1999, 68(41): 1089-1109.

[4] Chung J, Kang NC, Lee JM. A study on free vibration of a spinning disk. Journal of Mechanical Science and Technology, 1996, 10(2): 138-145.

[5] Farag NH, Pan J, Modal characteristics of in-plane vibration of circular plates clamped at the outer edge, Journal of the Acoustical Society of America, 2003, 113: 1935–1946.

[6] Ambati G, Bell JFW, Sharp JCK. In-plane vibrations of annular rings. Journal of Sound and Vibration, 1976, 47(3): 415-432.

[7] Nigh GL, Olson MD. Finite element analysis of rotating disks. Jouranl of Sound and Vibration, 1981, 77(1): 61-78.

[8] Park CI. Frequency equation for the in-plane vibration of a clamped circular plate. Journal of Sound and Vibration 2008, 313; pp: 325-333.

[9] Bshmal S, Bhat R, Rakheja S. In-plane free vibration of circular annular disks. Journal of Sound and Vibration, 2009, 322(1-2): 216-226.
[10] T. Irie, G. Yamada, Y. Muramoto, Natural frequencies of in-plane vibration of annular plates, Journal of Sound and Vibration 97(1984) 171–175.
[11] Tornabene F. Free vibration analysis of functionally graded conical, cylindrical shell and annular plate structures with a four-parameter power-law distribution. Computer Methods in Applied Mechanics and Engineering 2009; 198(37-40), pp: 2911-2935.
[12] Kermani ID, Ghayour M, Mirdamadi HR. Free vibration analysis of multi-directional functionally graded circular and annular plates. Journal of Mechanical Science and Technology 2012, 26(11), pp: 3399-3410.
[13] Nie GJ, Zhong Z. Semi-analytical solution for three-dimensional vibration of functionally graded circular plates. Computer Methods and Applied Mechanical Engineering 2007, 196; pp: 4901-4910.
[14] Dong CY. Three-dimensional free vibration analysis of functionally graded annular plates using the Chebyshev–Ritz method. Material and Design 2008, 29; pp: 1518-1525.
[15] Malekzadeh P, Shahpari SA, Ziaee HR. Three-dimensional free vibration of thick functionally graded annular plates in thermal environment. Journal of Sound and Vibration 2010, 329; pp: 425-442.
[16] Yang Y, Kou KP, Iu VP, Lam CC, Zhang C. Free vibration analysis of two-dimensional functionally graded structures by a meshfree boundary–domain integral equation method. Composite Structures 2014;110(0):342-353.
[17] Gao XW, Zhang C, Sladek J, Sladek V. Fracture analysis of functionally graded materials by a BEM. Composites Science and Technology 2008;68(5):1209-1215.
[18] Gao XW, Davies TG. Boundary Element Programming in Mechanics. Cambridge University Press; 2002.
[19] Gao XW. The radial integration method for evaluation of domain integrals with boundary-only discretization. Engineering Analysis with Boundary Elements 2002;26(10):905-916.
[20] Golberg MA, Chen CS, Bowman H. Some recent results and proposals for the use of radial basis functions in the BEM. Engineering Analysis with Boundary Elements 1999;23(4):285-296.
[21] Yang Y, Lam CC, Kou KP, Iu VP. Free vibration analysis of the functionally graded sandwich beams by a meshfree boundary-domain integral equation method. Composite Structures 2014;117(0):32-39.
[22] Yang Y, Lam CC, Kou KP, Iu VP. Free vibration analysis of two-dimensional functionally graded coated and undercoated substrate structures. Engineering Analysis with Boundary Elements 2015;60:10-17.
[23] Yang Y, Lam CC, Kou KP, Iu VP. Forced vibration analysis of functionally graded beams by the meshfree boundary-domain integral equation method. Engineering Analysis with Boundary Elements 2016;72:100-110.